Colloid Polym Sci (2005) 283: 393–401
DOI 10.1007/s00396-004-1158-4

ORIGINAL CONTRIBUTION

Tsuneo Okubo
Hiroshi Kimura
Hiromi Hase
Peter A. Lovell
Nicola Errington
Supranee Thongnoi

Colloidal crystals of core–shell-type spheres in deionized aqueous suspension

Received: 28 November 2003
Accepted: 12 April 2004
Published online: 22 June 2004

T. Okubo (✉) · H. Kimura · H. Hase
Department of Applied Chemistry and Graduate School of Materials Science, Gifu University, Yanagido 1-1, 501-1193 Gifu, Japan
E-mail: okubotsu@apchem.gifu-u.ac.jp
Fax: +81-58-293-2628

P. A. Lovell · N. Errington · S. Thongnoi
Manchester Materials Science Centre, UMIST, Manchester, M1 7HS, UK

Abstract The structure, crystal growth kinetics and rigidity of colloidal crystals of core–shell-type latex spheres (diameters 280–330 nm) with differences in shell rigidity have been studied in aqueous suspension, mainly by reflection spectroscopy. The suspensions were deionized exhaustively for more than 2 years using mixed-bed ion-exchange resins. The five kinds of core–shell spheres examined form colloidal crystals, where the critical sphere concentrations, ϕ_c, of crystallization (or melting) are high and range from 0.01 to 0.06 in volume fraction. Nearest-neighbor intersphere distances in the crystal lattice agree satisfactorily with values calculated from the sphere diameter and concentration. The crystal growth rates are between 0.1 and 0.3 s^{-1} and decrease slightly as the sphere concentration increases, indicating that the crystal growth rates are from the secondary process in the colloidal crystallization mechanism, corresponding to reorientation from metastable crystals formed in the primary process and/or Ostwald-ripening process. The rigidities of the crystals range from 2 to 200 Pa, and increase sharply as the sphere concentration increases. The *g* factor, the parameter for crystal stability, is around 0.02 irrespective of the sphere concentration and/or the kind of core–shell sphere. There are no distinct differences in the structural, kinetic and elastic properties among the colloidal crystals of the different core–shell-type spheres, showing that the internal sphere structure does not affect the properties of the colloidal crystals. The results show that colloidal crystals form in a closed container owing to long-range repulsive forces and the Brownian movement of colloidal spheres surrounded by extended electrical double layers and that their formation is not influenced by the rigidity and internal structure of the spheres.

Keywords Core–shell sphere · Colloidal crystal · Rigidity · *g* factor

Introduction

Crystal-like distributions of colloidal particles in suspension, i.e., colloidal crystals, form in a closed container owing to long-range repulsive forces and the Brownian movement of the colloidal particles surrounded by extended electrical double layers [1, 2, 3, 4, 5, 6, 7, 8, 9, 10]. The structural and kinetic properties of colloidal crystals are influenced strongly by the shape, size distribution and surface charge density of the spheres, the degree of deionization of the suspension, and the interaction of the colloidal spheres with the cell wall. With regard to the last factor, for example, the densest crystal planes, 111 and 100 planes for the

face-centered-cubic (fcc) and body-centered-cubic (bcc) lattices, respectively, always orient parallel to the cell wall [11]. Furthermore, colloidal crystallization rates are much higher for cells with planar walls than for tubular cells with curved walls [11].

Our previous work has reported important observations on the morphological properties of colloidal crystals. Giant colloidal crystals were discovered 10 years ago in studies of exhaustively deionized, extremely dilute aqueous suspensions of colloidal spheres of polystyrene and silica [12, 13, 14]. Various types of single crystals (crystallites) were observed through a metallurgical microscope [15, 16]. Poly(tetrafluoroethylene) spheres also formed giant colloidal crystals in aqueous suspension [17]. Giant single crystals formed even in the presence of simple electrolytes, polyelectrolytes and ionic detergents [18]. Large colloidal crystals also form in polar organic solvents and their aqueous mixtures when the solvents and the colloidal spheres are deionized thoroughly [19]. Recently, Yoshinaga and coworkers [20, 21, 22] succeeded in forming colloidal crystals from polymer-modified colloidal silica spheres in solvents of lower polarity, such as acetonitrile and benzene. Anisotropically shaped particles (e.g., rodlike, bowl-shaped and ellipsoidal) form three-dimensional ordered structures in suspension when the particle dimensions are highly monodisperse [23, 24, 25]. Recently, thermosensitive colloidal crystals were formed simply by mixing colloidal silica spheres with gel spheres of poly(*N*-isopropyl acrylamide) [26, 27]. Our studies on the thermodynamic and kinetic properties of colloidal crystals have been reviewed in several papers [10, 11, 16, 28, 29, 30].

Colloidal spheres that have internal structure are well known in the field of emulsion polymerization, the simplest being the core–shell type in which there is a core of one polymer surrounded by a concentric shell of a different polymer [31]. The term core–shell is often used more generically to include colloidal spheres that have several concentric layers. Even for the more complex core–shell spheres, the chemical and physical properties of the polymer in each layer are readily controlled through the synthesis procedures and the comonomers used to prepare the layer [31]. This paper reports on colloidal crystallization of several kinds of core–shell spheres, studied principally by reflection spectroscopy, with the objective of establishing whether the internal structure and rigidity of colloidal spheres influences colloidal crystallization.

Experimental

Materials

Two categories of core–shell spheres were used in the colloidal crystallization studies and were prepared in the form of latexes by monomer-starved semibatch emulsion polymerization procedures [31]. Details of the layer polymer compositions, the structures, and the diameters (d_o) of the core–shell spheres are given in Table 1. The values of d_o are *z*-average particle diameters measured by photon correlation spectroscopy at 25 ± 0.1 °C and 90° scattering angle using a series of 60-s scans on a Brookhaven instrument equipped with a 20-mW He–Ne laser and a BI-9000AT digital correlator; a minimum of 30 separate measurements were made for each diluted latex sample using the cumulants method for data analysis and the mean value of d_o was calculated.

Table 1 Structure and particle diameter information for the core–shell-type latex spheres. *PL1* comprises spheres with a simple core–shell structure, whereas *PL2–PL5* comprise spheres with three concentric layers: a core, an interlayer and a shell. The layers were prepared using the comonomer compositions shown: acrylic acid (*AA*); *n*-butyl acrylate (*BA*); ethyl acrylate (*EA*); hexan-1,6-diol diacrylate (*HDA*); methyl methacrylate (*MMA*); styrene (*S*); the *numbers* given in *parentheses* indicate the mole percent of comonomer used in the formation of the layer. The volume percent data are the percentages of the sphere volume associated with the layer

Latex	Sphere structure						d_o/nm
	Core		Interlayer		Shell		
	Composition	vol%	Composition	vol%	Composition	vol%	
PL1	BA (100)	5	–	–	BA (91) AA (9)	95	319
PL2	BA (100)	5	BA (61) AA (6) HDA (9)	40	BA (91) AA (9)	55	292
PL3	BA (100)	5	BA (58) AA (5) HDA (37)	40	BA (91) AA (9)	55	312
PL4	MMA (95) EA (5)	24	BA (78) S (22)	55	MMA (95) EA (5)	21	415
PL5	MMA (95) EA (5)	24	BA (78) S (22)	55	MMA (95) EA (5)	21	463

Latexes PL1–PL3 were prepared in accord with procedures reported for the preparation of core–shell pressure-sensitive adhesives [32]. Each of these types of core–shell spheres were prepared from a poly(*n*-butyl acrylate) seed latex formed in situ. PL1 spheres have a simple core–shell structure in which the seed latex was grown by formation of a poly[(*n*-butyl acrylate)-*co*-(acrylic acid)] shell. PL2 and PL3 spheres have three layers and were grown from the seed latex in two stages, firstly with cross-linked poly[(*n*-butyl acrylate)-*co*-(acrylic acid)] and then with non-cross-linked poly[(*n*-butyl acrylate)-*co*-(acrylic acid)]; they differ in terms of the level of cross-linking comonomer used in formation of the interlayer. Thus, the PL1–PL3 core–shell spheres have a similar rubbery shell of low glass-transition temperature ($T_g \approx -26$ °C by dynamic mechanical thermal analysis, DMTA) but an increasingly stiff internal rubbery phase due to the increase in the level of cross-linking in the rubbery interlayer.

Latexes PL4 and PL5 were prepared in accord with procedures reported for the preparation of acrylic toughening particles [33]. A poly[(methyl methacrylate)-*co*-(ethyl acrylate)] seed latex was formed in situ and grown directly in three stages: first by growth of the poly[(methyl methacrylate)-*co*-(ethyl acrylate)] seed to the required size, then by formation of a poly[(*n*-butyl acrylate)-*co*-(styrene)] interlayer, and finally by formation of a poly[(methyl methacrylate)-*co*-(ethyl acrylate)] shell. Thus, PL4 and PL5 spheres have a three-layer structure in which the shell and core are of a glassy polymer ($T_g \approx 119$ °C by DMTA), but the interlayer is a rubbery polymer ($T_g \approx 0$ °C by DMTA).

Exhaustive deionization is essential for studies of colloidal crystallization and requires a long period of treatment. The core–shell sphere latexes were deionized using a mixed bed of cation- and anion-exchange resins [Bio-Rad, AG501-X8 (D), 20–50 mesh] for a period of more than 2 years before use in the colloidal crystallization studies. They released small amounts of ionic impurities from their surfaces during this process.

Sample suspensions of the core–shell spheres were prepared by dilution of the deionized latexes with water in observation cells that contained cation- and anion-exchange resins and the samples were allowed to equilibrate over the resins for at least 1 month before measurements of colloidal crystallization were begun. The water used for the sample preparation was purified by a Milli-Q reagent grade system (Milli-RO5 plus and Milli-Q plus, Millipore, Bedford, MA).

Closeup color photography of colloidal single crystals

Photographs of colloidal crystals in a test tube were taken with a Canon EOS55 camera using a macro lens (EF50 mm, $f = 2.5$) and a life-size converter EF. Velvia film (Fujichrome, RVP135, ISO 50) was used for color transparencies. The light source was a pocket-type flashlight (BF-775, Xenon 4, National).

Dynamic light-scattering measurements

Dynamic light-scattering (DLS) measurements were made at 25 ± 0.02 °C with an Otsuka Electronics DLS-7000 spectrophotometer in a cylindrical vat containing silicone oil. A 5-mL sample suspension was prepared in a Pyrex tube cell (12-mm outside diameter and 130-mm length). Data analysis was carried out using the non-negative least squares and Marquardt methods [34].

Reflection spectroscopy

Reflection spectra of the sample suspensions were recorded at an incident angle of 90° through a Pyrex sample tube (NN-13, Maruemu Co., Osaka; 8-mL suspension volume, 10-mm inner diameter and 100-mm high) using an Otsuka Electronics MCPD-7000G3 multichannel photodetector connected to a Y-type optical fiber cable.

The crystal growth rate was measured from the growth of the peak in the reflection spectra with time after the sample suspensions had been mixed and left to stand still. The rigidities of the crystals were determined from reflection spectroscopy in sedimentation equilibrium [35, 36]. A sample suspension of 6-mL volume was introduced into the cell. About 0.5 mL of a mixed bed of ion-exchange resins [Bio-Rad, AG501-X8(D)] was added and the cells were then left to stand. The reflection spectra at various heights were recorded for 2 months using the photodetector.

Results and discussion

Morphology of colloidal single crystals

All the sample suspensions were milky, white and turbid, this being caused by the strong multiple scattering of the rather large spheres (around or over 300 nm in diameter). However, the samples also emitted strong iridescent colors and showed the presence of small single crystals (crystallites), confirming that they contained colloidal crystals [10, 11].

Typical closeup color pictures of the samples at sedimentation equilibrium are shown in Fig. 1. With the exception of PL1, the colloidal crystals are rather small. This is clearly because the sphere concentrations are high (0.012–0.09 in volume fraction) and the number of nuclei formed in the nucleation process is large. For PL1, however, large crystals ranging 0.1 to 2 mm were

observed. This indicates that the sphere concentration of the suspension in Fig. 1a is close to the critical sphere concentration of crystallization (or melting), ϕ_c.

Phase diagram

The value of ϕ_c ranged from 0.01 to 0.06 in the order PL1 ($\phi_c = 0.06$) > PL3 (0.04) > PL2 (0.016) > PL4 (0.012)~PL5 (0.01). These ϕ_c values are 2 orders of magnitude higher than the values typically observed ($\phi_c = 0.0002$) for colloidal crystals formed from polystyrene and silica spheres of 100-nm diameter. Previous studies have shown that ϕ_c values locate around 0.0002 irrespective of the sphere diameter in the range 100–200 nm [14]. The present studies are the first measurements of ϕ_c values for crystallization of colloidal spheres with diameters around or over 300 nm. It is clear, therefore, that above a certain size, the sphere diameter becomes an important factor in controlling the value of ϕ_c. There is, however, no direct correlation with d_o, which may be due to differences in polydispersity index. It should be noted that the ϕ_c values of PL4 and PL5, which contain no carboxylic groups, are much lower compared with those of PL1, PL2 and PL3, which have carboxylic acid groups. As is well established, a large number of simple ions distribute around the charged colloidal spheres, which are called electrical double layers. At low ionic concentrations, especially in the deionized state, the double layers are extended, and the electrostatic intersphere repulsion forces prevail to great distances on the order of micrometers. Thus, colloidal crystallization should take place quite easily at low concentrations of simple ions in suspension, and then ϕ_c should be lower for the spheres of lower charge densities.

Fig. 1 Closeup color photographs of colloidal crystals of PL1 (**a**, $\phi = 0.069$), PL2 (**b**, $\phi = 0.09$), PL3 (**c**, $\phi = 0.055$), PL4 (**d**, $\phi = 0.014$), and PL5 (**e**, $\phi = 0.012$) at 25 °C

Reflection spectroscopy

Typical examples of the reflection spectra of the suspensions are shown in Fig. 2. The sharp peaks show the presence of colloidal crystals in the suspensions. The lattice spacing, the nearest-neighbor intersphere distance, in fcc and bcc lattices ($l_{obs,f}$ and $l_{obs,b}$) are given by Eq. (1):

$$l_{obs,f} = l_{obs,b} = 0.6124\lambda p/n_s, \quad (1)$$

where λ_p denotes the wavelength of the primary reflection peak and n_s is the refractive index of the sample suspension, which was taken to be 1.333 at 25 °C for water, since the measurements were made at relatively low sphere concentrations. Many studies have reported that the fcc lattice is stabler than the bcc one, though the critical concentration for melting is sensitive to the degree of deionization of the suspension and also to the polydispersity of the spheres [10, 11].

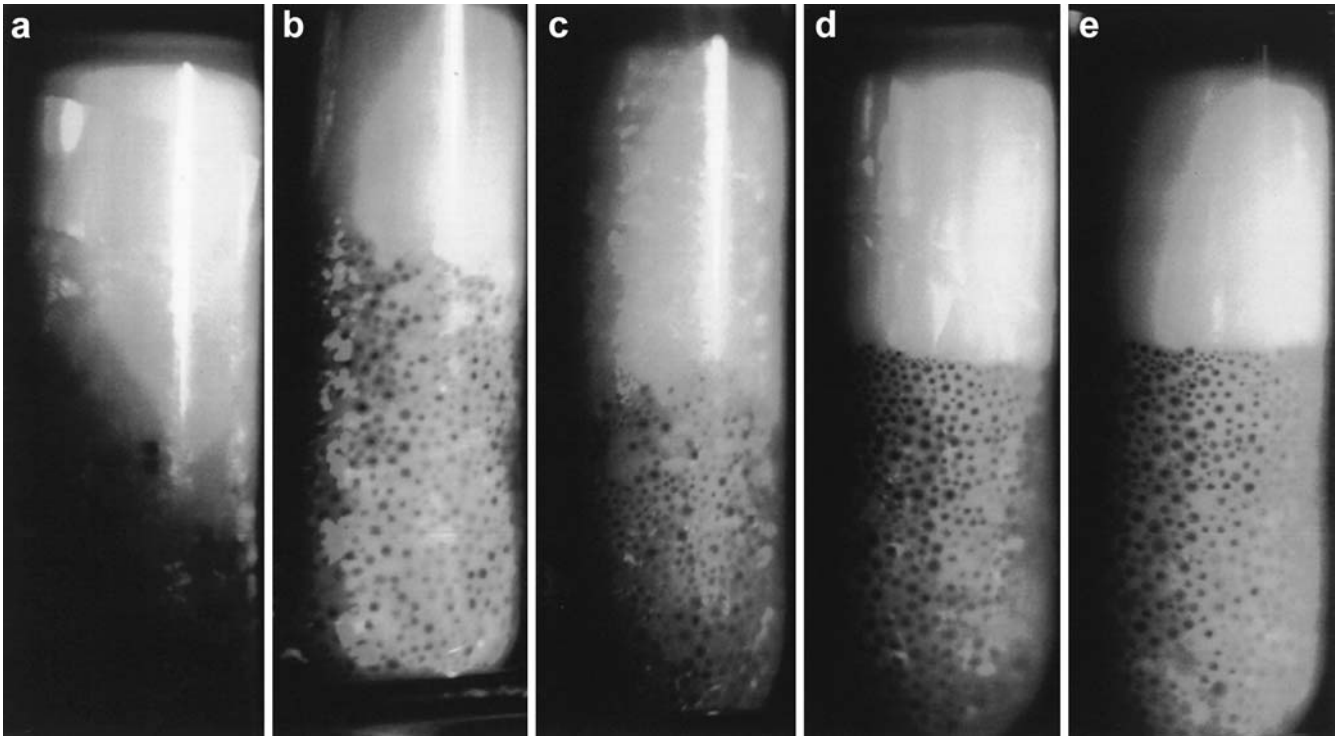

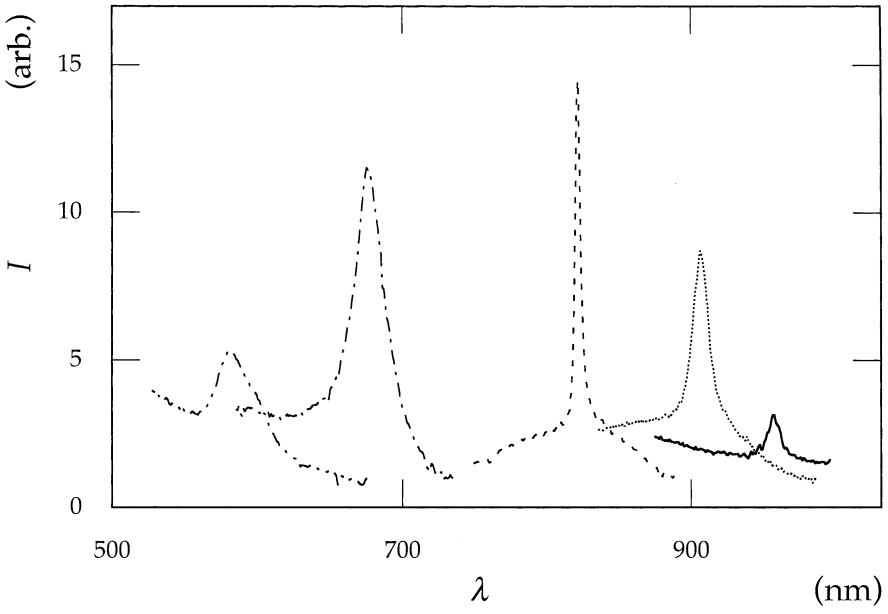

Fig. 2 Reflection spectra of PL3 suspension at 25 °C. $\phi = 0.025$ (*solid line*), $\phi = 0.03$ (*dotted line*), $\phi = 0.04$ (*dashed line*), $\phi = 0.08$ (*dash–dotted line*), $\phi = 0.12$ (*dash–double-dotted line*)

The lattice spacing calculated for a simple cubic lattice, l_o, is given by Eq. (2):

$$l_o = 0.904 d_o \phi^{-1/3}, \tag{2}$$

where d_o and ϕ are, respectively, the sphere diameter (in nanometers) and the volume fraction sphere concentration.

The nearest-neighbor intersphere distance, l_{obs}, is shown in Fig. 3 as a function of sphere concentration. Agreement with the calculation is excellent. It should be noted that the spectrophotometer used is able to scan wavelengths ranging from 350 to 1,000 nm, and that the observed peaks are secondary or tertiary peaks. The values for primary peaks are, therefore, calculated using the equation $\lambda_p = n\lambda_{obs}$, where n denotes the order of the peak observed. This method of calculation will contain relatively large experimental errors. Furthermore, experimental errors from uncertainty in the specific gravity of the spheres will not be negligible.

Analysis of crystallization kinetics

Typical changes in the reflection spectra during the course of crystallization are shown in Fig. 4. The size of colloidal single crystals from homogeneous nucleation,

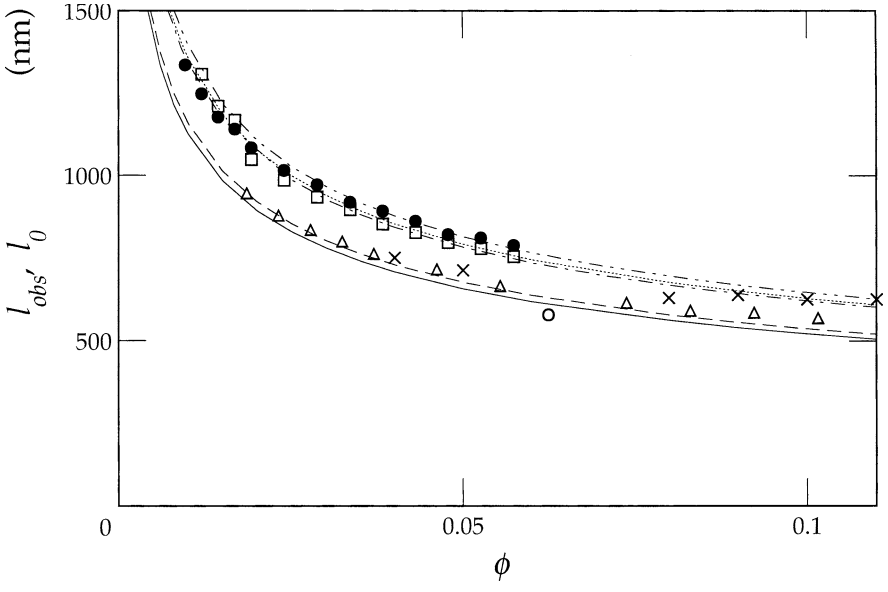

Fig. 3 Intersphere spacing of colloidal crystals observed (PL1 *open circles*, PL2 *crosses*, PL3 *triangles*, PL4 *squares*, PL5 *filled circles*) as a function of sphere concentration at 25 °C. Calculation: PL1 (*solid line*), PL2 (*dotted line*), PL3 (*dashed line*), PL4 (*dash–dotted line*), PL5 (*dash–double-dotted line*)

L, is evaluated from the peak intensity, I, in the reflection spectra [35, 36]:

$$I \cong N_{\text{cryst}} L^3 \cong L^3, \tag{3}$$

where N_{cryst} is the number of single crystals in the reflecting volume, which is directly proportional to the number concentration of crystals in the final stages of the crystallization process, being equal to the total number of nuclei formed over the full period of crystallization.

Typical traces of the peak intensity and the peak wavelength for PL3 spheres in the course of crystallization are shown in Fig. 5. The intensity increased as time increased and saturated to a constant value. On the same timescale, the wavelength rapidly decreased and quickly reached a consistent value. These results indicate that the observed changes in intensity and wavelength correspond to the secondary crystallization step, where metastable and loose crystals formed in the first step become stabler and more compact [36].

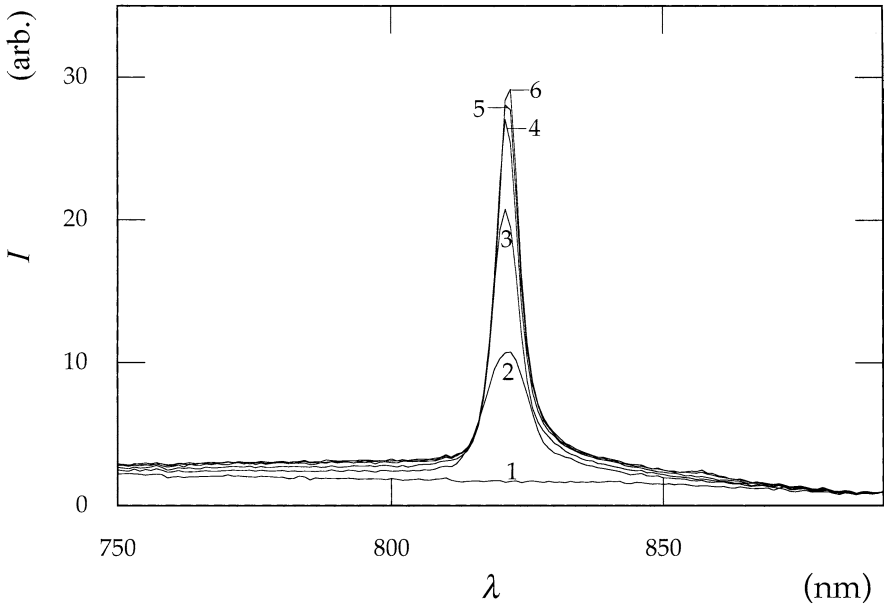

Fig. 4 Reflection spectra of PL3 ($\phi = 0.04$) suspension at 25 °C. Time after sample setting: 0 s (*1*), 228 s (*2*), 588 s (*3*), 1,188 s (*4*), 1,788 s (*5*), 2,388 s (*6*)

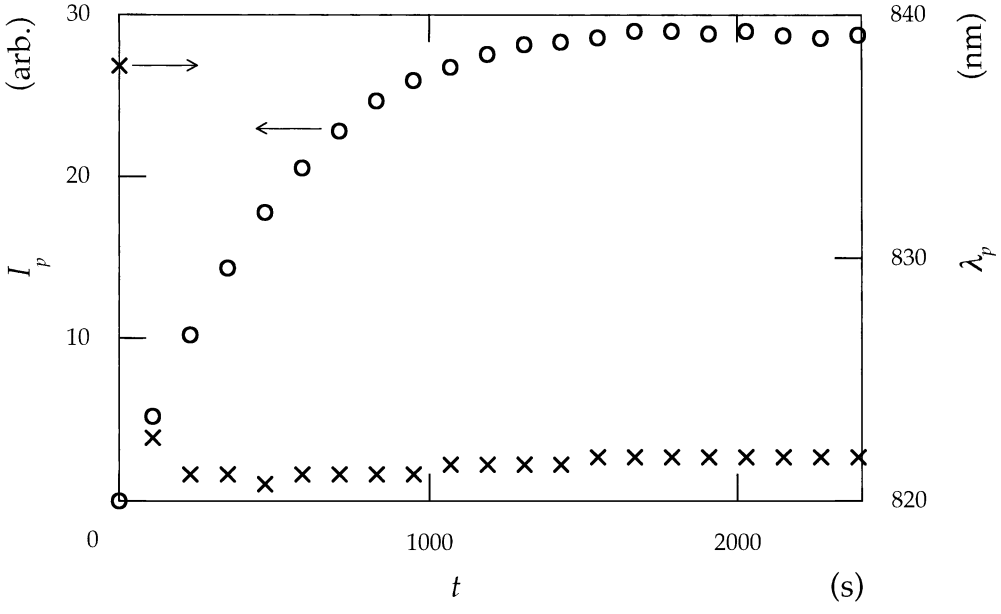

Fig. 5 Peak intensity (*circles*) and the peak wavelength (*crosses*) for PL3 ($\phi = 0.04$) suspension during the course of crystallization at 25 °C

Rigidity of the crystals

An example of how the reflection peak wavelength varies with height in the cell under conditions of sedimentation equilibrium 55 days after the sample suspension was set is shown in Fig. 6. For sedimentation equilibrium Eq. (4) holds [37]:

$$\lambda_p - \lambda_{p,m} = \left(p_{eff} g_o \lambda_{p,m} \phi_m / G\right)(h - h_m), \quad (4)$$

where $\lambda_{p,m}$ and ϕ_m are, respectively the peak wavelength and the volume fraction sphere concentration at the mid-plane of the cell, h_m, ϕ_m is the initial volume fraction sphere concentration, ρ_{eff} is the effective density given by the specific gravity of the spheres minus that of the solvent, g_o is the gravitational constant, h is the height from the bottom of the cell, and G is Young's elastic modulus for the colloidal crystals (or crystal rigidity) and is obtained by applying Eq. (4) to the slopes of λ_p versus h plots (such as that shown in Fig. 6). The linearity of the λ_p versus h plots was satisfactory for all the suspensions measured.

The crystal rigidities, G, thus obtained are shown in Fig. 7 as a function of the logarithm of the sphere

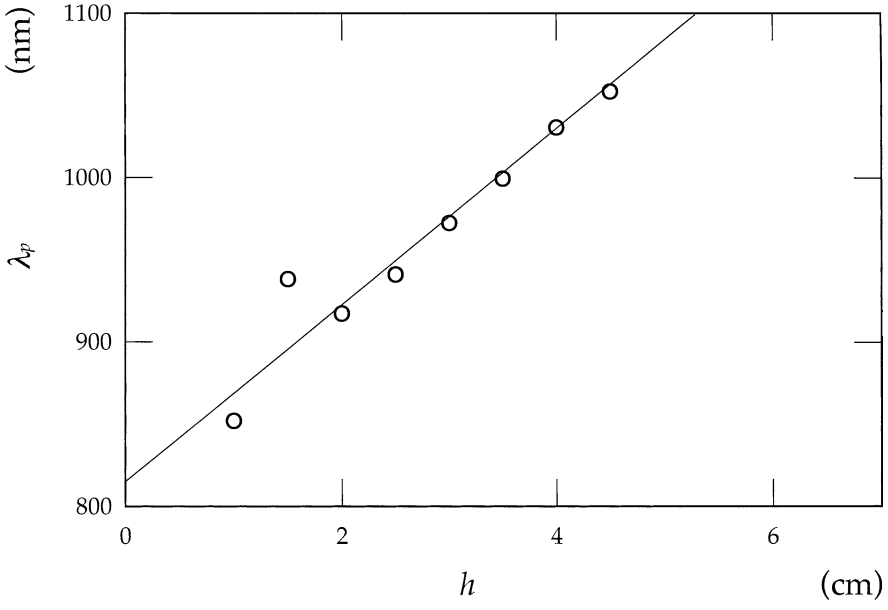

Fig. 6 Peak wavelength as a function of cell height in sedimentation equilibrium 55 days after the suspension had been set for PL3 ($\phi = 0.02$) spheres at 25 °C

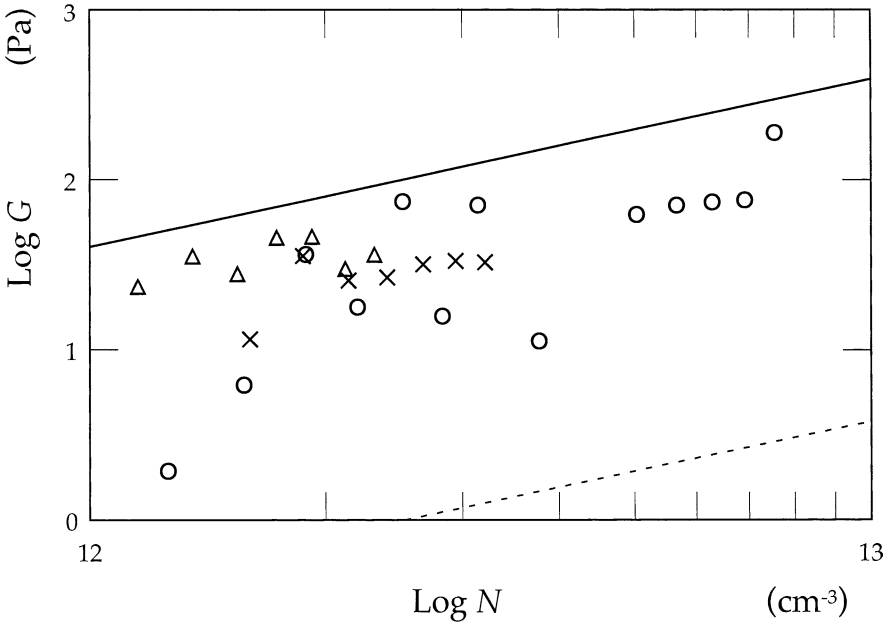

Fig. 7 Log G at 25 °C as a function of log N. PL3 (*circles*); PL4 (*crosses*); PL5 (*triangles*); $g = 0.01$ (*solid line*); $g = 0.1$ (*dashed line*)

Table 2 Parameters (25 °C) for colloidal crystals of core–shell-type PL3–PL5 latex spheres

Latex	ϕ	$N/10^{12}$ cm^{-3}	k/s^{-1}	G/Pa	g
PL3	0.020	1.26	0.17	1.9	0.052
	0.025	1.57	0.16	6.2	0.032
	0.030	1.89	0.087	36	0.015
	0.035	2.20	0.22	18	0.022
	0.040	2.52	0.15	74	0.012
	0.045	2.83	0.21	16	0.027
	0.050	3.14	0.16	71	0.014
	0.060	3.77	0.22	11	0.038
	0.080	5.03	0.32	62	0.018
	0.090	5.66	0.23	71	0.018
	0.100	6.29	0.21	74	0.019
	0.110	6.92	0.19	76	0.019
	0.120	7.55	–	189	0.013
PL4	0.060	1.60	0.22	11	0.024
	0.070	1.87	0.25	36	0.015
	0.080	2.14	0.22	26	0.018
	0.090	2.40	0.22	27	0.019
	0.100	2.67	0.15	32	0.019
	0.110	2.94	0.045	33	0.019
	0.120	3.20	0.15	33	0.020
PL5	0.040	0.77	–	10	0.018
	0.050	0.96	–	14	0.017
	0.060	1.15	0.29	23	0.014
	0.070	1.35	0.28	35	0.013
	0.080	1.54	0.15	28	0.015
	0.090	1.73	0.16	45	0.013
	0.100	1.92	0.08	46	0.013
	0.110	2.12	0.17	30	0.017
	0.120	2.31	0.18	36	0.016

concentration given by the number density of spheres, N. In general, G is written in terms of the magnitude of the thermal fluctuations of a sphere as [38, 39]

$$G \cong f/l \cong \left(k_{\mathrm{B}}T/\langle\delta_T^2\rangle\right)/l, \tag{5}$$

where f is the force constant between colloidal spheres, δ_{T} is the thermal fluctuation of a sphere in the effective potential valley, k_{B} is the Boltzmann constant, and T is the suspension temperature. Introducing a nondimensional parameter, g, for $\langle\delta_{\mathrm{T}}^2\rangle^{1/2}/l$, we obtain the rigidity as a linear function of the number density of spheres, N:

$$G \cong Nk_{\mathrm{B}}T/g^2. \tag{6}$$

The solid and broken lines in Fig. 7 show the rigidities calculated from Eq. (6) when $g = 0.01$ and 0.1, respectively. Lindemann's law of crystal melting informs us that $g < 0.1$ holds for a stable crystal. The g values cited in Table 2 were about 0.02 irrespective of the sphere concentration and/or the kind of spheres.

Conclusions

In conclusion, there were no distinct differences in the kinetic and elastic properties among the colloidal crystals of the different types of core–shell spheres. Hence, the evidence from the present studies is that several characteristic parameters of colloidal core–shell spheres, such as molecular components, mechanical properties and surface properties, do not play an important role for colloidal crystallization. Since colloidal crystals are formed by long-range repulsive forces through the Brownian movement of spheres surrounded by extended electrical double layers, this observation is entirely plausible. Of course, the size, its distribution, charge density and sphere concentration are important for colloidal crystallization of all kinds of colloidal spheres, including the core–shell-type spheres studied in this work.

Acknowledgements The Ministry of Education, Science, Sports and Culture, Japan is thanked for grants-in-aid for Scientific Research on Priority Area (A) (11167241) and for Scientific Research (B) (11450367). Financial support from the UK Engineering and Physical Sciences Research Council and Rhodia Specialties (for N.E.) and from the Thai Government and Ineos Acrylics (for S.T.) is gratefully acknowledged. T.O. appreciates deeply the late Prof. Emeritus Sei Hachisu for his continual encouragement and comments on our work.

References

1. Vanderhoff W, van de Hul HJ, Tausk RJM, Overbeek JTG (1970) In: Goldfinger G (ed) Clean surfaces: their preparation and characterization for interfacial studies. Dekker, New York
2. Hiltner PA, Papir YS, Krieger IM (1971) J Phys Chem 75:1881
3. Kose A, Ozaki M, Takano K, Kobayashi Y, Hachisu S (1973) J Colloid Interface Sci 44:330
4. Mitaku S, Ohtsuki T, Kishimoto A, Okano K (1980) Biophys Chem 11:411
5. Lindsay HM, Chaikin PM (1982) J Chem Phys 76:3774
6. Pieranski P (1983) Contemp Phys 24:25
7. Ottewill RH (1985) Ber Bunsenges Phys Chem 89:517
8. Aastuen DJW, Clark NA, Cotter LK, Ackerson BJ (1986) Phys Rev Lett 57:1733
9. Pusey PN, van Megen W (1986) Nature 320:340
10. Okubo T (1988) Acc Chem Res 21:281
11. Okubo T (1997) Curr Top Colloid Interface Sci 1:169
12. Okubo T (1992) Naturwissenschaften 79:317
13. Okubo T (1993) Colloid Polym Sci 271:190
14. Okubo T (1994) Langmuir 10:1695
15. Okubo T (1987) Ber Bunsenges Phys Chem 91:516
16. Okubo T (1994) In: Schmitz KS (ed) Macro-ion characterization for dilute solutions to complex fluids. American Chemical Society, Washington, DC

17. Okubo T, Yoshimi H, Shimizu T, Ottewill RH (2000) Colloid Polym Sci 278:474
18. Okubo T, Fujita H, Kiriyama K, Yamaoka H (1996) Colloid Polym Sci 274:73
19. Okubo T (1994) Langmuir 10:3529
20. Yoshinaga K, Chiyoda M, Ishiki H, Okubo T (2002) Colloids Surf 204:285
21. Okubo T, Ishiki H, Kimura H, Chiyoda M, Yoshinaga K (2002) Colloid Polym Sci 280:290
22. Okubo T, Ishiki H, Kimura H, Chiyoda M, Yoshinaga K (2002) Colloid Polym Sci 280:446
23. Okubo T (1987) Angew Chem Int Ed Engl 26:765
24. Okubo T, Aotani S (1988) Colloid Polym Sci 266:1049
25. Okubo T, Aotani S (1988) Naturwissenschaften 75:145
26. Okubo T, Hase H, Kimura H, Kokufuta E (2002) Langmuir 18:6783.
27. Okubo T (2003) Sen'i Gakkaishi 59:43 (in Japanese)
28. Okubo T (1993) Prog Polym Sci 18:481
29. Stoimenova M, Okubo T (1999) In: Schwarz JA, Contescu CI (eds) Surfaces of nanoparticles and porous materials. Dekker, New York, p 103
30. Okubo T (2002) In: Hubbard A (ed) Encyclopedia of surface and colloid science. Dekker, New York, p 1300
31. Lovell PA, El-Aasser MS (eds) (1997) Emulsion polymerization and emulsion polymers. Wiley, Chichester
32. Garrett J, Lovell PA, Shea AJ, Viney RD (2000) Macromol Symp 151:487
33. Lovell PA, McDonald J, Saunders DEJ, Young RJ (1993) Polymer 34:61
34. Okubo T, Kiriyama K, Nemoto N, Hashimoto H (1996) Colloid Polym Sci 274:93
35. Dhont JKG, Smits C, Lekkerkerker HNW (1992) J Colloid Interface Sci 152:386
36. Okubo T, Ishiki H (2000) J Colloid Interface Sci 228:151
37. Crandall RS, Williams R (1997) Science 198:293
38. Mitaku S, Ohtsuki T, Kishimoto A, Okano K (1980) Biophys Chem 11:411
39. Okubo T (1989) J Chem Soc Faraday Trans 1 85:455